Optical Properties of (100)- and (111)-Oriented GaInAs/GaAs Strained-Layer Superlattices

B. K. Laurich,[1] K. Elcess,[2],[a] C. G. Fonstad,[2] J. G. Beery,[1] C. Mailhiot,[3] and D. L. Smith[1]
[1]*Los Alamos National Laboratory, Los Alamos, New Mexico 87545*
[2]*Massachusetts Institute of Technology, Cambridge, Massachusetts 02139*
[3]*Xerox Webster Research Center, Webster, New York, 14580*
(Received 8 July 1988; revised manuscript received 6 December 1988)

We have studied the optical properties of GaInAs/GaAs strained-layer superlattices grown along the [100] and [111] crystallographic axes. Absorption and luminescence spectra for the two superlattices show qualitatively different behavior. These differences are attributed to the presence of strain-generated electric fields in the (111) strained-layer superlattice, which have been predicted theoretically but have not been previously observed experimentally.

PACS numbers: 78.65.Fa, 73.20.Dx, 78.55.Cr

It is now well established that strained-layer superlattices (SLS's) can be grown with a high degree of crystalline perfection.[1-3] For sufficiently thin layers, the lattice-constant mismatch is accommodated by internal strains rather than by the formation of dislocations. To date, virtually all SLS's have been grown along the [100] axis. A new effect in SLS's with a [111] growth axis has been predicted: large internal electric fields generated by the piezoelectric effect.[4] Such strain-generated electric fields are not expected in (100) superlattices.[4] Theoretical arguments suggest that these internal electric fields should substantially change the electronic structure and optical properties[5] of (111) SLS's and lead to large nonlinear optic[6] and electro-optic effects.[7] The fields cause a tilting of the energy bands and lead to a red shift of optical transition energies and changes in oscillator strengths. In this Letter, we present a comparative study of the optical properties of (100) and (111) $Ga_{1-x}In_xAs/GaAs$ SLS's. We show that the lowest-energy intrinsic transition shifts to the red by about 20 meV in the (111) sample. The spectra of this sample can be fitted only by including the strain-generated electric fields. These results give strong evidence for the presence of the strain-generated electric fields in (111) SLS's and are the first observation of physical consequences of these fields.

The strain-generated electric fields are the principal difference expected between (100) and (111) superlattices. Only small quantitative changes in the electronic structure and optical properties are expected due to anisotropies in effective masses, deformation potentials, etc.[5] Recent experimental work on the lattice-matched $Ga_{1-x}Al_xAs/GaAs$ system, where strain-generated electric fields do not occur, has borne out these expectations.[8] Absorption spectra for these lattice-matched (100) and (111) superlattices are very similar. There is a one-to-one correspondence between absorption peaks, and the strength of corresponding transitions are very nearly the same. Thus, if one neglects the strain-generated electric fields, one expects (100) and (111) superlattices to behave very similarly.

We investigated two $Ga_{1-x}In_xAs/GaAs$ SLS samples grown simultaneously by molecular-beam epitaxy on semi-insulating GaAs substrates. One sample was grown on a (100) substrate and the other on a (111) *B* substrate. Details of the growth procedure have been described previously.[9] Each superlattice consisted of twenty periods of 70 Å of the $Ga_{1-x}In_xAs$ well and 140 Å of the GaAs barrier. Secondary-ion-mass spectroscopy profiling was used for layer thickness characterization. Within the accuracy of the measurements (about 10%) the periods of the two superlattices were the same and were equal to the value expected from the growth calibrations. Rutherford backscattering was used for composition characterization. The In composition in the two samples was similar and given by $x=0.10\pm0.02$. The superlattices were grown on a 3000-Å graded buffer of GaInAs. Thus, we expect a "free standing" superlattice with the thinner GaInAs wells strained approximately twice as much as the GaAs barriers. The samples were not intentionally doped. However, there was carbon incorporation at about the 10^{15}-cm^{-3} level, so that the superlattices were lightly *p* type.

Figure 1 shows the absorption spectra of the (100) and (111) samples taken at 4.2 K. The arrows mark the peaks of the main intrinsic luminescence lines observed in the two samples. The strong-absorption threshold at $\lambda\sim832$ nm in both samples is due to the substrate and/or buffer. In the (100) sample, two principal absorption features are seen. These features show up as steps. Excitonic effects are not pronounced in these spectra. The luminescence lines occur at the absorption threshold and are shifted to lower energy with respect to the midpoint of the absorption step. In the (111) sample, three principal absorption features are seen. Again, these features show up as absorption turnons rather than excitonic peaks and the luminescence lines occur at the absorption thresholds.

Figure 2 shows a luminescence spectrum from the (100) sample and two spectra from the (111) sample. These spectra are representatives of a large data set taken at temperatures between 4.2 and 150 K and excitation

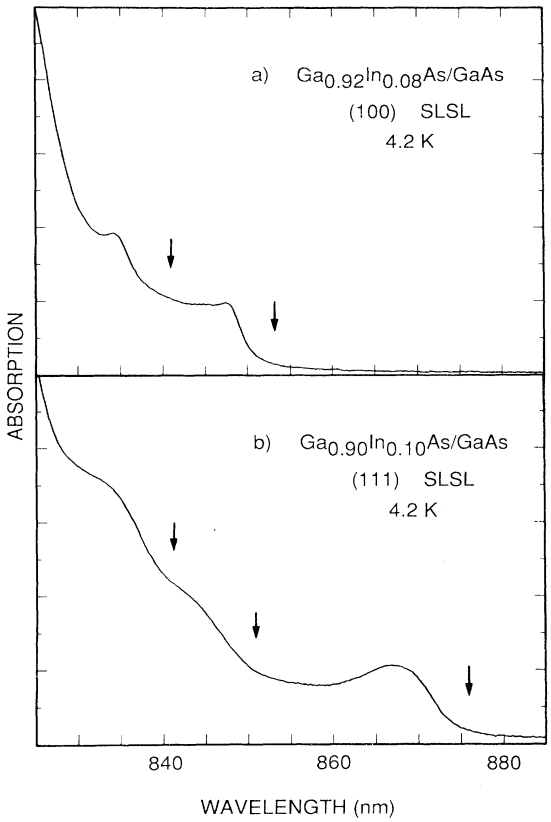

FIG. 1. Optical-absorption spectra of $Ga_{1-x}In_xAs/GaAs$ superlattices oriented (a) along the [100] axis, and (b) along the [111] axis. The corresponding position of intrinsic luminescence lines are marked.

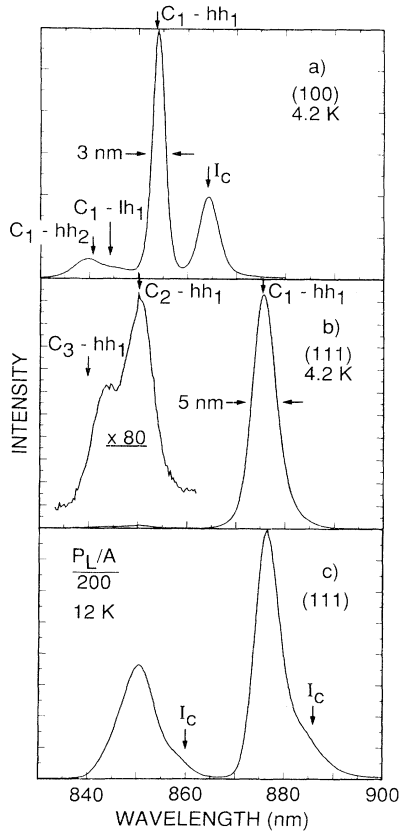

FIG. 2. Luminescence spectra of (a) (100) oriented SLS, (b) (111) oriented SLS at 4.2 K and 50 W/cm^2, and (c) (111) oriented SLS at 12 K and 0.25 W/cm^2. The calculated positions of intrinsic transitions are indicated.

intensities between 1 mW/cm^2 and 100 W/cm^2. The arrows labeled C_1-hh_1, etc. correspond to calculated energy positions for intrinsic transitions. Features that we attribute to impurity transitions are labeled I_c. These arrows do not correspond to calculated results.

The spectrum in Fig. 2(a) was taken at 4.2 K and an excitation intensity of 0.3 W/cm^2. The peaks at 854 and 841 nm correspond to absorption features, whereas the peak at 864 nm does not. We attribute the peak at 854 nm to a C_1-hh_1 transition, the peak at 864 nm to a C_1 to an acceptor (probably carbon) transition, and the peak at 841 nm primarily to the C_1-lh_1 transition. The zone-center lh_1 state is just slightly above the zone-center hh_2 state, and they strongly admix and share oscillator strength away from the zone center. We believe that the admixing of these two bands causes the somewhat unusual line shape of the 841-nm peak. The transition energy of the 864-nm line is about 16 meV lower than the C_1-hh_1 line. The 16-meV difference in transition energies is reasonably close to the expected binding energy of an acceptor near the well-barrier interface.[10] The excitation and temperature dependence of the intensities of the three lines are consistent with the above assignments. The 841-nm line is most prominent at low temperatures and higher excitation. This line (C_1-lh_1) corresponds to a transition in which the hole is an excited state. The holes are not in thermal equilibrium. The intersubband relaxation occurs via acoustic-phonon scattering. At higher temperatures this scattering rate increases, the number of photoinjected holes remaining in the excited level decreases, and the 841-nm luminescence line decreases in intensity. At very low excitation, where the density of photoinjected holes is much less than the density of doped-in holes in the hh_1 state, the excited-state transition at 841 nm vanishes.

The spectrum in Fig. 2(b) was taken at 4.2 K and an excitation intensity of 50 W/cm^2 and that in Fig. 2(c) at 12 K and 0.25 W/cm^2. Each of the three lines in the spectrum of Fig. 2(b), at 876, 851, and 842 nm, corresponds to a feature in the absorption spectrum. We attribute the 876-nm line to a C_1-hh_1 transition, the 851-nm line to a C_2-hh_1 transition, and the 842-nm line to a C_3-hh_1 transition. In Fig. 2(c), the 876- and 851-nm lines have developed low-energy shoulders separated

from the main peak by about 10 nm (16 meV). We attribute the low-energy shoulders on the 876- and 851-nm lines to C_1 and C_2 to acceptor transitions, respectively. The two shoulders have the same temperature and excitation dependence. They saturate at high intensity and lose intensity at temperatures greater than about 30 K. This behavior is consistent with impurity-related transitions. The shoulders on the 876- and 851-nm lines strongly support the identification of the 851-nm line as a C_2-hh_1 transition.

Luminescence measurements at 4.2 K show that the dependence of the intensity ratio I(851 nm):I(876 nm) in the (111) sample on excitation power is opposite to that of the ratio I(841 nm):I(851 nm) in the (100) sample. At 50-W/cm^2 excitation, the intensity ratio (851 nm:876 nm) is 1:80, whereas at 1 mW/cm^2, this ratio is 2:1. This intensity dependence shows that the 851-nm line cannot correspond to a transition involving an excited hole state. At the lowest excitation, 1 mW/cm^2, the density of photoinjected holes, which can persist in an excited state, is significantly lower than the density of doped-in holes, which are in the hh_1 ground state.[11] Since the 851-nm line is more intense than the 876-nm line at low intensities, it must correspond to a transition involving an excited electron. The excitation dependence of the 842-nm line follows that of the 851-nm line, and so this transition must also involve a hole in the hh_1 ground state and an excited electron.

We have performed a series of electronic structure calculations on free-standing (100) and (111) $Ga_{1-x}In_xAs/GaAs$ superlattices using the method of Ref. 12. We fixed the $Ga_{1-x}In_xAs$ thickness at 70 Å, the GaAs thickness at 140 Å, and adjusted the composition to give the transition energies for the C_1-hh_1 transitions. This gave $x=0.08$ for the (100) sample and $x=0.10$ for the (111) sample. These values are consistent with the Rutherford backscattering composition measurements. On the basis of Ref. 13, we take the average valence-band offset independent of orientation and strain conditions. We find $\langle \Delta E_v \rangle = 0.2x$ eV. This value is somewhat larger than that reported in Refs. 14 and 15, equal to that in Ref. 16, and smaller than that in Ref. 17. Our results and interpretation are not strongly dependent on the choice of valence-band offset. Other input parameters are the same as in Ref. 5.

In Fig. 3, we show calculated energy-band diagrams for one well and two barriers for the (100) superlattice [(a)], the (111) superlattice neglecting the internal electric fields [(b)], and the (111) superlattice, including the internal electric fields [(c)]. The calculated energy positions of the lowest electron and hole states, relative to the band edges, are also shown. For states with significant dispersion along the growth axis, the bandwidth for k in this direction is indicated.

In the conduction band of the (100) superlattice, only the C_1 state is confined in the wells. The C_2 level starts a three-dimensional continuum. The superlattice is

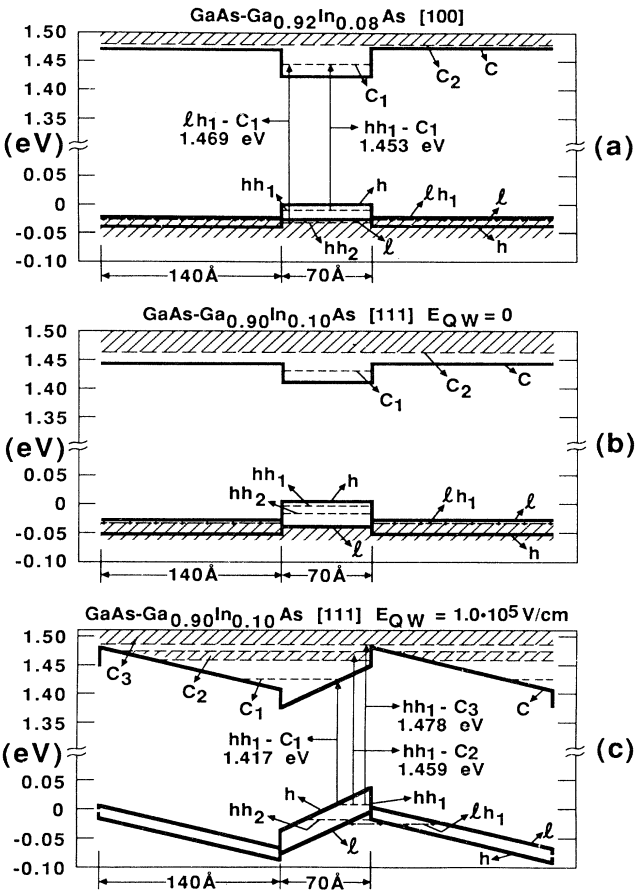

FIG. 3. Calculated energy-band diagrams and electronic-state energies for (a) (100) oriented SLS, (b) (111) oriented SLS, neglecting strain-generated electric fields, and (c) (111) oriented SLS, including strain-generated electric fields.

slightly type II for light holes. Even the lowest-energy light-hole state is essentially unconfined. The lh_1 state is slightly higher in energy than the hh_2 state at the zone center, and there is strong admixture of these two bands slightly away from the zone center. The results for the (111) superlattice neglecting the internal fields are very similar to those for the (100) superlattice. The sloping band edges in Fig. 3(c) are due to the electric fields (1.0×10^5 V/cm in the well and half this value in the barrier). Note, the electric fields have qualitatively changed the electronic structure compared to the results of Figs. 3(a) and 3(b). For example, the C_2 states are now confined by the triangular potential due to the internal electric fields.

The experimental results on the (100) sample are well described by the calculations shown in Fig. 3(a). The results on the (111) sample cannot be even qualitatively interpreted in terms of the calculations of Fig. 3(b), which neglect the strain-induced electric fields. Those calculations give results which are almost the same as for

the (100) sample and would predict similar behavior, whereas we observe qualitatively different behavior for the two samples. However, the experimental results on the (111) sample are well described by the calculations shown in Fig. 3(c), in which the internal electric fields are included.

In summary, we have presented a comparative study of the optical properties of GaInAs/GaAs SLS's grown along (100) and (111). These results give strong evidence for the presence of strain-generated electric fields in (111) SLS's having a magnitude predicted by elastic theory.[4]

We gratefully acknowledge the secondary-ion-mass spectroscopy measurements by Gerald Nelson and Mark Paffett of Sandia and Los Alamos National Laboratories, respectively. The work of B.K.L., J.G.B., and D.L.S. has been supported by Los Alamos National Laboratory Internal Supporting Research. The work of K.E. and C.G.F. has been supported by the National Science Foundation through the Massachusetts Institute of Technology Center for Materials Science and Technology, Grant No. DMR 84-18718.

---

[a]Present address: Centre National d'Etudes des Télécommunications, 196 rue Henri Ravera, 92220 Bagneux, France.

[1]J. W. Matthews and A. E. Blakeslee, J. Cryst. Growth **27**, 118 (1974), and **29**, 273 (1975), and **32**, 265 (1976).

[2]G. C. Osbourn, R. M. Biefeld, and P. L. Gourley, Appl. Phys. Lett. **41**, 172 (1982).

[3]I. J. Fritz, L. R. Dawson, and T. E. Zipperian, Appl. Phys. Lett. **43**, 846 (1983).

[4]D. L. Smith, Solid State Commun. **57**, 919 (1986).

[5]C. Mailhiot and D. L. Smith, Phys. Rev. B **35**, 1242 (1987).

[6]D. L. Smith and C. Mailhiot, Phys. Rev. Lett. **58**, 1264 (1987).

[7]C. Mailhiot and D. L. Smith, Phys. Rev. B **37**, 10415 (1988).

[8]T. Hayakawa, K. Takahashi, M. Kondo, T. Suyama, S. Yamamoto, and T. Hijikata, Phys. Rev. Lett. **60**, 349 (1988).

[9]K. Elcess, J. L. Lievin, and C. G. Fonstad, J. Vac. Sci. Technol. B **6**, 638 (1988).

[10]W. T. Masselink, Y. C. Chang, and H. Morkoc, Phys. Rev. B **32**, 5190 (1985); Y. C. Chang, Physica (Amsterdam) **146B**, 137 (1987).

[11]The carrier lifetime has not been measured in this sample. But even assuming a very long lifetime of 10 ns, the density of photoinjected holes, at 1 mW/cm^2, is over 2 orders of magnitude less than the doping density.

[12]D. L. Smith and C. Mailhiot, Phys. Rev. B **33**, 8345 (1986); C. Mailhiot and D. L. Smith, Phys. Rev. B **33**, 8360 (1986).

[13]C. G. Van de Walle and R. M. Martin, Phys. Rev. B **34**, 5621 (1986).

[14]T. G. Andersson, Z. G. Chen, V. C. Kulakovskii, A. Uddin, and J. T. Vallin, Phys. Rev. B **37**, 4032 (1988).

[15]J. Y. Marzin, M. N. Charasse, and B. Sermage, Phys. Rev. B **31**, 8298 (1985).

[16]I. J. Fritz, B. L. Doyle, T. J. Drummond, R. M. Biefeld, and G. C. Osbourn, Appl. Phys. Lett. **48**, 1606 (1986).

[17]J. Menendez, A. Pinczuk, D. J. Werder, S. K. Sputz, R. C. Miller, D. L. Sivco, and A. Y. Cho, Phys. Rev. B **36**, 8165 (1987).